International Journal of Pharmaceutics 477 (2014) 613–622

Contents lists available at ScienceDirect

International Journal of Pharmaceutics

journal homepage: www.elsevier.com/locate/ijpharm

PEGylated mesoporous silica as a redox-responsive drug delivery system for loading thiol-containing drugs

Qinfu Zhao [a], Chen Wang [b], Ying Liu [b], Jiahong Wang [c], Yikun Gao [d], Xiaojing Zhang [b], Tongying Jiang [a], Siling Wang [a,*]

[a] Department of Pharmaceutics, School of Pharmacy, Shenyang Pharmaceutical University, 103 Wenhua Road, Shenyang, Liaoning Province 110016, PR China
[b] Department of Pharmaceutical Chemistry, School of Pharmaceutical Engineering, Shenyang Pharmaceutical University, PR China
[c] Department of Physiology, School of Life Science and Biopharmaceutics, Shenyang Pharmaceutical University, PR China
[d] School of Medical Devices, Shenyang Pharmaceutical University, PR China

ARTICLE INFO

Article history:
Received 6 August 2014
Received in revised form 17 October 2014
Accepted 26 October 2014
Available online 31 October 2014

Keywords:
Colloidal mesoporous silica
Redox-responsive
6-Mercaptopurine
Methoxy polyethylene glycols
Disulfide bonds

ABSTRACT

In this paper, we describe the development of a redox-responsive delivery system based on 6-mercaptopurine (6-MP)-conjugated colloidal mesoporous silica (CMS) *via* disulfide bonds. mPEG was modified on the surface of silica to improve the dispersibility and biocompatiblity of CMS by reducing hemolysis and protein adsorption. The CMS carriers with different amounts of thiol groups were prepared to evaluate the impact of modified thiol on the drug loading efficiency. *In vitro* release studies demonstrated that the CMS nanoparticles exhibited highly redox-responsive drug release. The cumulative release of 6-MP was less than 3% in absence of GSH, and reached more than 70% within 2 h in the presence of 3 mM GSH. In addition, by comparing the cumulative release profiles of CMS-SS-MP@mPEG with their counterparts without the grafting of hydrophilic PEG, it was found that mPEG chains did not hinder the drug release due to the cleavable disulfide bonds and the improved dispersibility. Overall, this work provides a new strategy to connect thiol-containing/thiolated drugs and hydrophilic polymers to the interior and exterior of silica *via* disulfide bonds to obtain redox-responsive release and improve the dispersibility and biocompatibility of silica.

1. Introduction

Over the past twenty years, a great deal of work has been carried out on the development of targeted delivery systems, aimed to improve treatment efficacy and reduce the significant side effects of toxic anticancer drugs (Langer, 1998; Soppimath et al., 2001). However, although considerable progress has been made, few targeted delivery systems have obtained optimal effects, and this is generally due to premature drug release before reaching the target site. Therefore, the development of stimuli-responsive drug delivery systems (DDS) for cancer treatment has received widespread attention in recent years. Stimuli-responsive materials could safely deliver drug molecules to specific-target sites without degradation or premature release. This property is particularly important for drugs which are toxic or whose therapeutic dosage demands precise control. Stimuli-responsive DDS can involve a variety of stimuli such as changes in pH (Kim et al., 2010; Lee et al., 2010; Chen et al., 2013), reducing agents (Chen et al., 2013; Wang et al., 2013), enzymes (Park et al., 2009), temperature, and light (He et al., 2012). It is generally accepted that the concentration of glutathione (GSH) between extracellular fluids (2–20 μM) and intracellular fluids (1–10 mM) is significantly different (Cheng et al., 2011). Moreover, the cytosolic GSH levels in most tumor cells are at least 4-fold higher than those in normal cells (Saito et al., 2003). Hence, the advantage of using disulfide bonds which are cleavable at a high concentration of GSH is their relative stability in extracellular fluids and plasma, and breakdown in intracellular fluid.

Compared with traditional organic polymers or lipid-based nanoparticles (Torchilin, 2005), mesoporous silica nanoparticles (MSN) are regarded as an excellent stimuli-responsive carrier owing to their high surface area, large pore volume, excellent biocompatibility and chemical stability, tunable pore size, and easily modified surface (Zhao et al., 2010). The easily functionalized surface facilitates assembly of different moieties. In recent years, strategies based on drugs conjugated onto carriers, such as MSN and polymer or lipids materials, by stimuli-responsive bonds have been developed to achieve a 'zero premature release' ability (Lee et al., 2010; Duan et al., 2013; Wang et al., 2013). In this study, we describe the development of a redox-responsive DDS with the

* Corresponding author. Tel.: +86 24 23986348; fax: +86 24 23986348.
E-mail address: silingwang@syphu.edu.cn (S. Wang).

http://dx.doi.org/10.1016/j.ijpharm.2014.10.056
0378-5173/

drug covalently grafted onto MSN by disulfide bonds. Although only a limited number of drugs have a mercapto group, some drugs (such as doxorubicin or cisplatin) can undergo thiol grafting by a simple modified process, and then be covalently grafted to MSN by disulfide bonds (Ahn et al., 2013; Wang et al., 2013).

Most silica based stimuli-responsive DDS employ mesoporous MCM-41 as a drug carrier due to its two dimensionally ordered hexagonal pores and small particle size (Lai et al., 2003; Giri et al., 2005). However, the morphology of MCM-41 might become rod-like when the internal pores of the silica nanoparticles are modified with thiol groups by the co-condensation method (Möller et al., 2007). Also, the aggregation of thiol-functionalized MCM-41 is even more marked than that before modification. Therefore, the morphology and aggregation of thiol-functionalized MCM-41 is an important problem to be considered when intravenous administration is planned. In addition, GSH-triggered drug delivery can only release drug after the nanopartilces are internalized by cells. In addition, the smaller particles with a higher dispersibility under physiological conditions will be endocytosed with a higher efficiency than the larger particles (Zhao et al., 2010). Lu et al. have studied the effect of nanoparticle size on the cellular uptake of silica, indicating that the uptake is particle-size-dependent and the maximum uptake by HeLa cells occurs at a nanoparticle size of 50 nm (Lu et al., 2009). Therefore, it is highly desirable to develop novel thiol-functionalized nanosized mesoporous silica with a particle size of ca. 50 nm and excellent monodispersity as a redox-responsive drug carrier.

The extensive protein adsorption to the outer surface of DDS under physiological conditions and the recognition of silica as a foreign invader by the reticuloendothelial system (RES) will result in the rapid clearance of MSN from the circulation when administered intravenously (Gu et al., 2012). Hence, to take full advantage of the redox-responsive release properties, the circulation life of the MSN *in vivo* needs to be prolonged. Strategies based on surfaces grafted with poly(ethylene glycol) (PEG) have been developed to improve the dispersibility and prolong the circulation time of nanoparticle (He et al., 2010). PEGylated MSN has several advantages including resistance to proteolysis, increased blood circulation time, decreased immunogenicity, and excellent biocompatibility (Wang et al., 2010).

In the present study, stable suspensions of thiol-functionalized colloidal mesoporous silica (CMS) were prepared by the use of a cationic surfactant cetyltrimethylammonium chloride (CTACl) and triethanolamine (TEA) according to the literature (Möller et al., 2007). A novel drug-conjugated mesoporous CMS redox-responsive DDS was developed and 6-mercaptopurine (6-MP), an antimetabolite drug with a thiol group, was used as a model drug. Then, mPEG was grafted to the external surface of MSN by disulfide bonds in order to extend the circulation time and increase the dispersibility of the DDS. The hydrophilic mPEG chains were cleaved by GSH and did not hinder drug release due to the cleavable disulfide bonds. In addition, CMS reacting with different amounts of 3-mercaptopropyltrimethoxysilane (MPTMS) was prepared to evaluate the impact of thiol modification on the loading efficiency and release behavior of the drug. Overall, the study describes a new strategy to connect bioactive molecules and PEG to silica interiors and exteriors through disulfide bonds to obtain redox-responsive drug release.

2. Experimental

2.1. Materials

Tetraethoxysilane (TEOS), triethanolamine (TEA), cetyltrimethylammonium chloride (CTACl) were obtained from Tianjin Bodi Chemical Holding Co., Ltd. (Tianjin, China). 3-mercaptopropyltrimethoxysilane (MPTMS, 95%), 2,2′-dipyridyl disulphide, 3-mercaptopropionicacid, 6-mercaptopurine (6-MP), *N*-(3-dimethylaminopropyl)-*N*-ethylcarbodiimide hydrochloride (EDC), methoxy polyethylene glycols (mPEG, 5000), *N*-hydroxysuccinimide (NHS), and glutathione (GSH) were obtained from Sigma–Aldrich Chemical (Shanghai, China). All other chemicals were of analytical grade as required and used without further purification.

2.2. Preparation of thiol-functionalized CMS

The thiol-functionalized CMS nanoparticles were synthesized according to the published method with some modification (Möller et al., 2007). Briefly, 64 mL water, 10.5 mL ethanol, and 10.4 mL 25 wt% CTACl were stirred at room temperature for 10 min. This was followed by the addition of 4.125 mL TEA and further stirring until dissolution was complete. This solution (40 mL) was heated to 60 °C in a water bath, with the dropwise addition of a mixture of 2.9 mL TEOS and 0.25 ml MPTMS under stirring. After stirring for 2 h, the obtained nanoparticles were homogenized on a homogenizer at 800 bars for 5 cycles to reduce the aggregation of nanoparticles (AH100D, ATS Engineer Inc., Shanghai, China). Finally, the resulting product was centrifuged, washed with distilled water and ethanol for three times and dried under vacuum for 12 h. Different thiol-modified CMS carriers were prepared by regulating the volume of MPTMS added. The added volume of MPTMS was 0.25 ml, 0.5 mL, 0.75 mL, and 1 mL, while the volume of TEOS remained constant. The thiol-functionalized CMS samples were referred to as CMS-SH, CMS-2SH, CMS-3SH, and CMS-4SH. To remove the surfactant template CTACl, the solids were refluxed twice in a solution of 9 mL HCl (37%) and 160 mL methanol for 12 h, and then the surfactant-free samples were centrifuged, washed and dried under vacuum for 12 h.

2.3. Synthesis of 2-carboxyethyl 2-pyridyl disulphide (Py—SS—COOH)

2,2′-Dipyridyl disulphide (3.3 g) was dissolved in 20 mL tetrahydrofuran (THF) followed by the addition of 20 mL $NaHCO_3$ solution (0.03 M). The solution was then stirred vigorously and 10 mL THF solution containing 3-mercaptopropionic acid (1.06 g) was added dropwise to the mixture. The reaction mixture was stirred for 4 h, and THF was then removed by evaporation (Eyela Rotary Evaporator, Tokyo Rikakikai, Japan). The remaining aqueous phase was washed three times with 50 mL dichloromethane (DCM), and precipitation was carried out by adjusting the pH of the solution to 2–3. Then, the precipitate was extracted three times with 25 mL ethyl acetate (EA). The EA extract was evaporated and 20 mL $NaHCO_3$ solution was used to dissolve the product. Finally, a white product was obtained by adjusting the pH to 2–3.

2.4. Synthesis of CMS—SS—COOH

The thiol-functionalized CMS samples (500 mg) without template extraction were first suspended in ethanol (25 mL) then Py—SS—COOH (200 mg) was added. The mixture was stirred at room temperature for 24 h and then CMS—SS—COOH was collected by centrifugation and washed thoroughly with ethanol and water. The product was refluxed with hydrochloric acid in methanol at 80 °C for 12 h to remove the template CTACl.

2.5. Drug loading process

Firstly, 100 mg 6-MP was dissolved in 7 mL dimethylsulfoxide (DMSO) to obtain a yellow transparent solution and then 3 mL iodine solution was added dropwise to oxidize the mercaptopurine. The mixture was stirred at room temperature for 24 h and

then 200 mg CMS—SS—COOH was added to the mixture under an N_2 atmosphere to minimize air oxidation, followed by stirring at room temperature for another 24 h to allow the disulfide bond exchange reaction to take place. The resulting nanoparticles were centrifuged, washed with DMSO and ethanol, and dried under vacuum for 12 h. To prolong the circulation time and improve the dispersibility of the nanoparticles, mPEG was grafted onto the external surface of the carriers by esterification. Briefly, 100 mg 6-MP loaded CMS—SS—COOH was dispersed in 20 mL DMSO, and EDC (3 mg mL^{-1}) and NHS (2 mg mL^{-1}) were added to the mixture to activate the COOH for 1 h. Then, 50 mg mPEG was added to the solution, followed by stirring at room temperature for another 24 h. The resulting product was centrifuged, washed with DMSO and ethanol, and dried under vacuum for 12 h. The different thiol-functionalized CMS samples, CMS-SH, CMS-2SH, CMS-3SH, and CMS-4SH, after the drug loading process and grafting mPEG were referred to as CMS-SS-MP@mPEG-1, CMS-SS-MP@mPEG-2, CMS-SS-MP@mPEG-3, and CMS-SS-MP@mPEG-4, respectively. The mPEG modified CMS-2SH blank carrier by disulfide bonds was named as CMS-SS-mPEG-2 and prepared to evaluate the biocompatibility and BSA adsorption in the following sections. The preparation method was as follows. 200 mg CMS-SS-COOH-2 was dispersed in 20 mL DMSO, and activated by EDC and NHS for 1 h. Then, 50 mg mPEG was added and further stirred at room temperature for 24 h.

In order to prove that grafting mPEG to the out layer of the carrier through the cleavable disulfide bonds does not affect the release of 6-MP, thiol-functionalized CMS was directly reacted with 6-MP in iodine solution after the template extraction. The different thiol-functionalized CMS samples directly reacted with 6-MP after the template extraction were named CMS-SS-MP-1, CMS-SS-MP-2, CMS-SS-MP-3, and CMS-SS-MP-4, respectively.

The CMS-SH after template extraction was chosen as the drug carrier to load 6-MP by the adsorption equilibrium method (noncovalent interaction) to be used as a control to evaluate the redox-responsive release. The 6-MP loaded CMS-SH sample was named CMS-SH/MP. In order to measure the 6-MP payload of the silica carriers, ca. 10 mg of the MP-loaded samples was dispersed in 100 mL hydrochloric acid (pH 1.2). Then, sufficient GSH was added to the solution to ensure complete breakage of the disulfide bonds. The concentration of 6-MP was measured by UV–vis spectrophotometry (UV-2000, Unico, USA) at a wavelength of 320 nm.

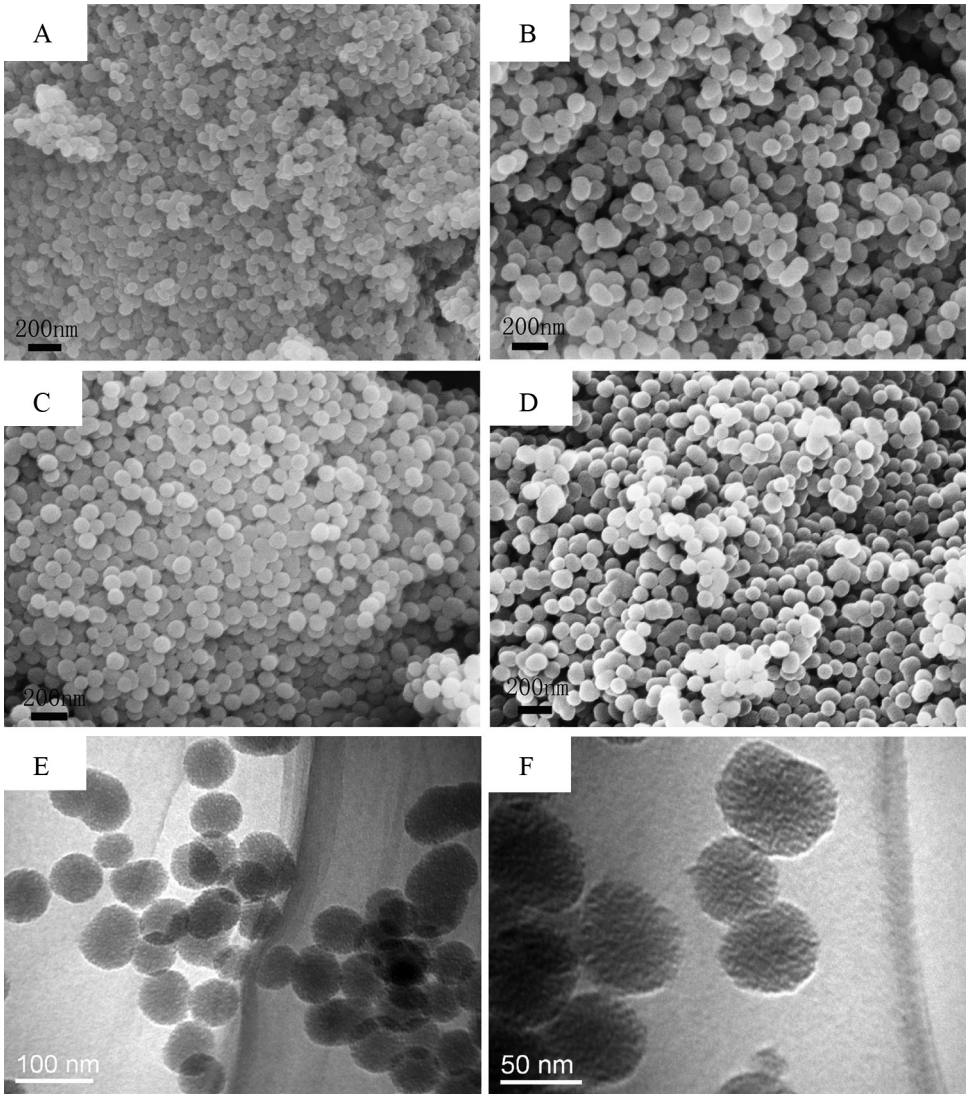

Fig. 1. SEM images of thiol-functionalized CMS nanoparticles (A) CMS-SH, (B) CMS-2SH, (C) CMS-3SH, and (D) CMS-4SH. TEM images of (E) and (F) CMS-SH.

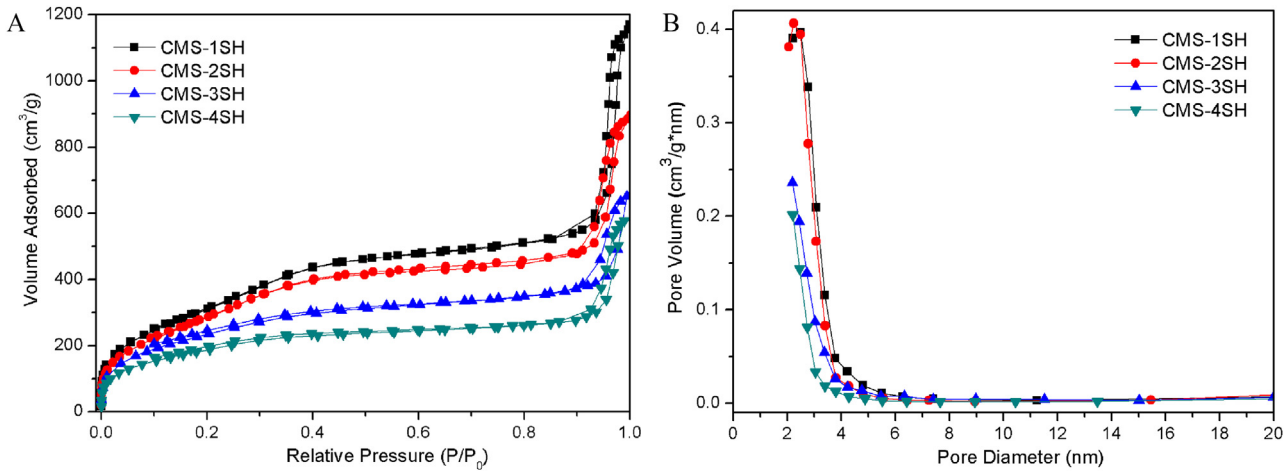

Fig. 2. The nitrogen adsorption–desorption isotherms (A) and pore size distributions (B) of thiol-functionalized CMS samples.

Table 1
The N_2 adsorption–desorption parameters and 6-MP loading efficiencies of different functionalized CMS nanoparticles.

Sample[a]	Addition volume of MPTMS (mL)	S_{BET}[a] (m^2/g)	Vt[b] (cm^3/g)	W_{BJH}[c] (nm)	Sample names after 6-MP loading	Drug loading (%)
CMS-SH	0.25	1185	1.70	2.5	CMS-SS-MP-1	3.28 ± 0.54
CMS-2SH	0.50	1109	1.29	2.2	CMS-SS-MP-2	4.95 ± 0.36
CMS-3SH	0.75	878	1.01	<2	CMS-SS-MP-3	4.10 ± 0.26
CMS-4SH	1.00	697	0.89	<2	CMS-SS-MP-4	2.73 ± 0.08
CMS-SS-COOH-1	0.25	970	1.44	2.5	CMS-SS-MP@mPEG-1	2.70 ± 0.20
CMS-SS-COOH-2	0.50	945	1.00	2.2	CMS-SS-MP@mPEG-2	4.07 ± 0.29
CMS-SS-COOH-3	0.75	790	0.89	<2	CMS-SS-MP@mPEG-3	2.78 ± 0.29
CMS-SS-COOH-4	1.00	701	0.74	<2	CMS-SS-MP@mPEG-4	2.02 ± 0.19

[a] S_{BET} is the B–E–T surface area calculated at a relative pressure of P/P_0 from 0.05 to 0.25.
[b] Vt is the total pore volume measured at a relative pressure of 0.98.
[c] W_{BJH} is the pore size distribution calculated by the B–J–H method on the desorption branches of the nitrogen isotherms.

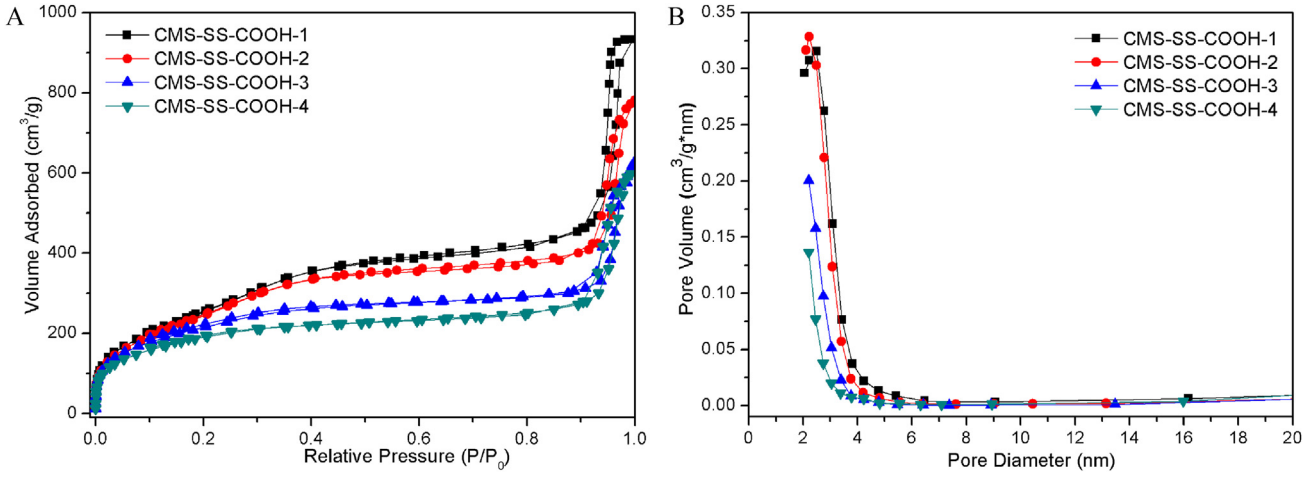

Fig. 3. The nitrogen adsorption–desorption isotherms (A) and pore size distributions (B) of CMS-SS-COOH samples.

2.6. Redox-triggered drug release

The redox-triggered release was carried out in a pH 7.4 phosphate buffer solution (PBS) (KC-8D, Tianjin Guoming Medical Equipment Co., Ltd., China). Release studies were carried out at 37 ± 0.5 °C with a paddle speed of 75 ± 1 rpm. 15 mg 6-MP loaded samples were dispersed in 100 mL PBS medium at zero time. Aliquots (4 mL) of the release medium were withdrawn at appropriate intervals and passed through a 0.22 μm membrane filter. In addition, an equal volume of fresh release medium was

Table 2
Surface elemental composition of thiol-functionalized CMS samples.

Sample	Atomic percentage (%)		
	Si 2p	O 1s	S 2p
CMS-SH	23.60	75.92	0.48
CMS-2SH	34.08	65.06	0.85
CMS-3SH	32.75	66.02	1.23
CMS-4SH	34.65	63.83	1.52

added immediately to keep the volume constant. The amount of released 6-MP was measured at a UV–vis detection wavelength of 320 nm. All measurements were carried out in triplicate.

2.7. Hemolysis assay

A hemolysis assay was used to evaluate the safety of CMS and CMS-SS-mPEG for *in vivo* applications. After collection of rabbit blood samples, red blood cells (RBCs) were collected by centrifugation at 1000 r/min for 10 min. The plasma supernatant was removed and the residual rabbit RBCs were washed three times with sterile isotonic saline. The residual RBCs were diluted to a concentration of 2% (v:v). Subsequently, 2% RBCs solutions were mixed with an equal volume of suspension solutions of carriers in saline, and the final concentrations of CMS-2SH and CMS-SS-mPEG-2 were 20, 50, 100, 200, 500, 1000, and 1500 μg/mL. The hemolysis of RBCs in saline and distilled water was used as a negative and positive control, respectively. The mixtures were allowed to stand for 4 h at room temperature and then centrifuged for 10 min at 1800 r/min and the upper clear fractions were measured at 541 nm using a UV–vis spectrophotometer.

Hemolysis percentage (%) = (absorbance of the sample − absorbance of the negative control)/(absorbance of the positive control − absorbance of the negative control) × 100.

2.8. BSA adsorption measurements

The protein adsorption to the surface of silica under physiological conditions was simulated by BSA adsorption measurements. The BSA adsorbance was determined according to the published method (He et al., 2010). For this, 90 mg BSA was completely dissolved in 150 mL distilled water under mild shaking. The prepared BSA solution was stored in a refrigerator at 4 °C. Phosphate buffered saline (0.15 M) was prepared by dissolving 4 g NaCl, 0.1 g KCl, 0.575 g Na_2HPO_4, and 0.1 g KH_2PO_4 in 500 mL distilled water, and stored at 4 °C. Then, 10 mg CMS-2SH and CMS-SS-mPEG-2 dispersed in 5 mL phosphate buffered saline, and then 5 mL BSA solution was added. The mixture obtained was placed in a shaker (37 °C) and shaken at 135 rpm. After 4 h, the mixed solutions were centrifuged, and the upper clear solutions were collected. The BSA solution was stained with Coomassie brilliant blue solution and the UV–vis absorption was measured at a wavelength of 595 nm. BSA adsorbed on CMS-2SH and CMS-SS-mPEG-2 were calculated using following equation:

$q = (Ci - Cf)V/m$, where Ci and Cf are the initial BSA and final BSA concentrations in solutions, before and after BSA adsorption, respectively; V is the total solution volume; m is the weight of nanoparticles added into the solution.

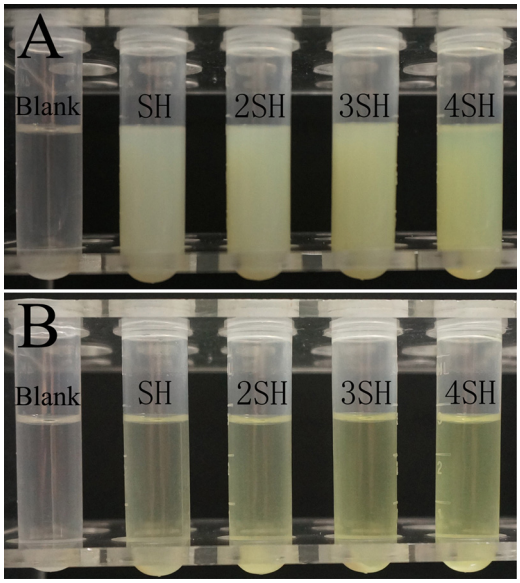

Fig. 4. The photographs of different thiol-functionalized CMS nanoparticles reacting with Py—SS—COOH in ethanol for 24 h with a silica concentration of 10 mg/mL (A) before centrifugation and (B) after centrifugation.

2.9. Characterization

Scanning electron microscopy (SEM) images were obtained using a field emission scanning electron microscope (ZEISS, SUPRA 35, Germany). Transmission electron microscopy (TEM) was performed on an FEI Tecnai G2 Microscope with an acceleration voltage of 200 kV. Particle size and zeta potential were measured on a Nano-zs90 Nanosizer (Malvern Instruments Ltd., UK), and the samples were dissolved in deionized water. Nitrogen adsorption analysis was measured at −196 °C on an adsorption analyzer (V-Sorb 2800P, China). The specific surface areas were calculated from the adsorption data using the Brunauer–Emmett–Teller (B–E–T) model, and the pore size was determined by the Barrett–Joyner–Halenda (B–J–H) method. All the samples were degassed at a suitable temperature under vacuum before measurements were carried out. X-ray photoelectron spectra were recorded using a high vacuum X-ray photoelectron spectroscope (ESCALAB250, Thermo VG, USA) with an Al-Kα X-ray source (hυ=n1486.6 eV). Fourier transform infrared (FT-IR) spectra were obtained on an FT-IR spectrometer (Bruker IFS 55, Switzerland) using the KBr pellet technique. The spectroscopic range was investigated from 400 cm^{-1} to 4000 cm^{-1}. The concentration of 6-MP in the solution was measured by UV–VIS spectrophotometry (UV-2000, Unico, USA) at a wavelength of 320 nm.

3. Results and discussion

3.1. Preparation and characterization of functionalized CMS

The thiol-functionalized CMS was synthesized by a co-condensation method to introduce thiol groups to the internal and external surfaces of CMS. This approach, depending on the simultaneous condensation of silicate precursors and MPTMS, was used in order to obtain a homogeneous distribution of thiol, but it requires a mild template extraction. Template extraction was performed twice with 9 mL HCl (37%) in 160 mL methanol at 80 °C for 12 h. The morphology and pore channel structures of the thiol-functionalized CMS nanoparticles were characterized by SEM and TEM. As shown in the SEM images (Fig. 1), all the prepared thiol-functionalized CMS nanoparticles, regardless of the amount of MPTMS added, were of a uniform spherical shape with a mean diameter of approximately 50–80 nm. Also, the mean diameter of thiol-functionalized CMS increased slightly when the volume of MPTMS added increased from 0.25 mL to 1 mL. Therefore, it could be concluded that the addition of MPTMS during the synthesis of thiol-modified CMS did not significantly affect the morphology of the carriers. TEM images of CMS-SH showed that most nanoparticles had a mean diameter of 50–70 nm (Fig. 1E and F). All nanoparticles were spherical in shape with a wormhole arrangement of the mesopores.

The B–E–T specific surface area (S_{BET}) and pore size distribution curves of thiol-functionalized CMS synthesized with different amounts of MPTMS were measured by N_2 adsorption–desorption analysis. The B–E–T isotherms and pore size distributions of thiol-functionalized CMS samples are shown in Fig. 2. The values of the S_{BET}, total pore volume (V_P) and B–J–H pore size distribution (W_{BJH}) of the corresponding samples are summarized in Table 1. The S_{BET},

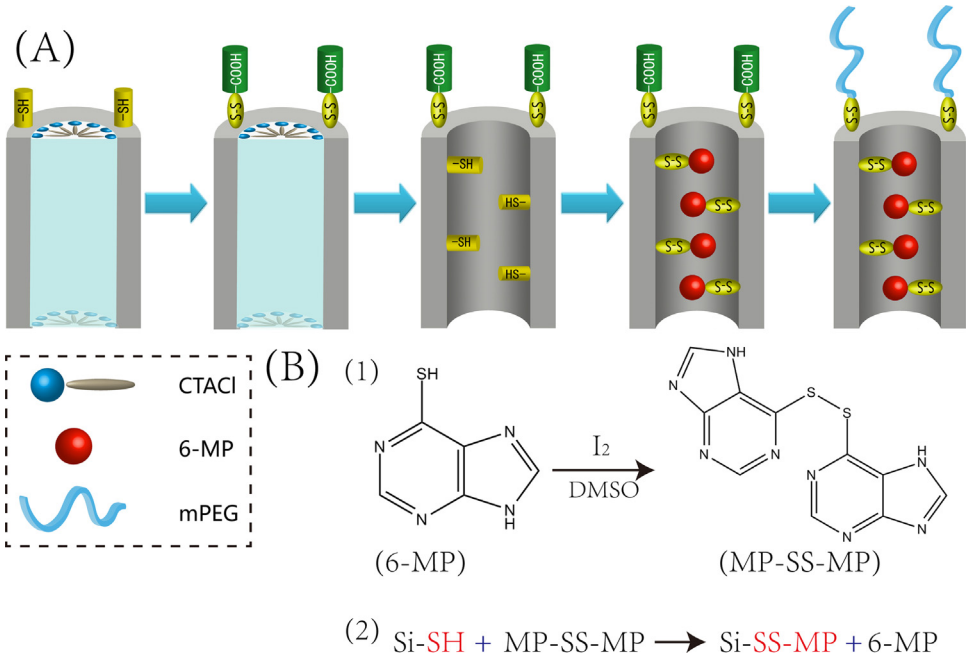

Scheme 1. (A) Drugs loading process for redox-responsive mesoporous CMS nanoparticles, and (B) drug loading mechanism by the disulfide bond exchange reaction.

V_P, and W_{BJH} of thiol-functionalized CMS gradually reduced on increasing the volume of MPTMS from 0.25 mL to 1 mL. CMS-SH had the highest S_{BET} up to 1185 cm^2/g, and the W_{BJH} was 2.5 nm. The CMS-2SH sample, prepared with the addition of 0.5 mL MPTMS, had a W_{BJH} of 2.2 nm. However, when the volume of MPTMS added increased to 0.75 mL or 1 mL, the W_{BJH} of thiol-functionalized CMS was reduced to the micropore range (<2 nm).

The B–E–T isotherms and pore size distribution curves of different CMS-SS-COOH samples are displayed in Fig. 3. The relevant N_2 adsorption–desorption parameters are also given in Table 1. The S_{BET} and V_P of CMS-SS-COOH samples were slightly reduced compared with thiol-functionalized CMS with the same degree of thiol modification due to the increased weight of 3-mercaptopropyltrimethoxy on the surface of the silica. Nevertheless, the W_{BJH} of CMS-SS-COOH samples did not significantly change compared with that of thiol-modified CMS, indicating that the internal pore network was not blocked after the grafting of SS-COOH on the surface of thiol-functionalized CMS.

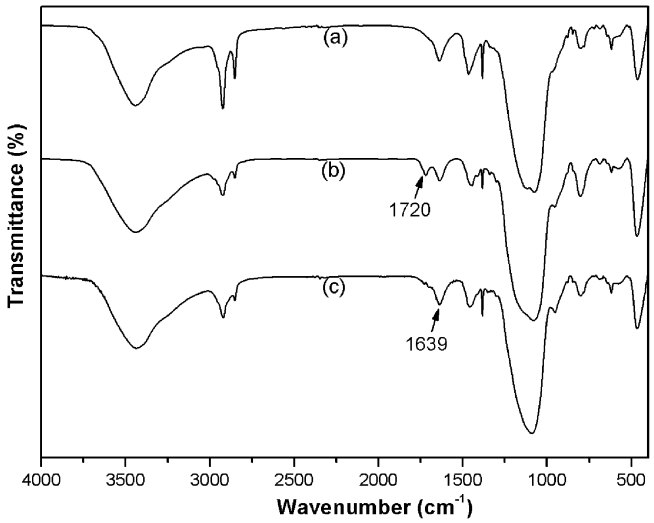

Fig. 5. The FT-IR spectra of CMS-2SH with template (a), CMS-SS-COOH-2 after template extraction (b), and CMS-SS-mPEG-2 (c).

X-ray photoelectron spectroscopy (XPS) was used to measure the elemental composition of the sample surfaces with an analysis depth of less than 10 nm. In the preparation of thiol-functionalized CMS, MPTMS was added to the surfactant solution by complete mixing with TEOS, so the mercapto group was grafted uniformly on the external and internal surfaces of the carrier. The elemental analysis results of the thiol-functionalized CMS nanoparticles, namely the Si, O, and S percentages, are shown in Table 2. The S percentage (%) increased markedly with addition of an increasing volume of MPTMS from 0.25 mL to 1 mL, indicating an increase in the thiol groups on the interior and exterior of CMS. The different amounts of modified thiol on the surface of CMS were also confirmed by the color change during the synthesis of CMS-SS-COOH. The reactant, 2-carboxyethyl 2-pyridyl disulphide, is colorless in ethanol, however the byproduct, mercaptopyridine, is yellow after the outside surface thiols of CMS were reacted converted to carboxylic acid. As shown in Fig 4, the color of the yellow reaction solution gradually became deeper from the sample CMS-SH to CMS-4SH, indicating the increased thiol groups on the surface of CMS. This result is consistent with the data obtained by XPS.

3.2. Drug loading and characterization

The drug loading procedure involved a combination of mercaptopurine oxidation and a disulfide bond exchange reaction. 6-MP was first oxidized to 1,2-di(purin-6-yl) disulfane (MP-SS-MP) by iodine, and then reacted with the thiol of CMS by a disulfide bond exchange reaction Scheme 1B. The mPEG was grafted onto the external surface of the carrier in order to prolong the circulation time and increase the dispersibility of DDS. However, the outer mPEG may influence the release of drug entrapped in the DDS (Cui et al., 2012). Taking this into account, in the present work, mPEG was grafted onto the surface of silica through cleavable disulfide bonds.

The drug loading process of redox-responsive CMS nanoparticles is shown in Scheme 1A. In this, mPEG and 6-MP were both

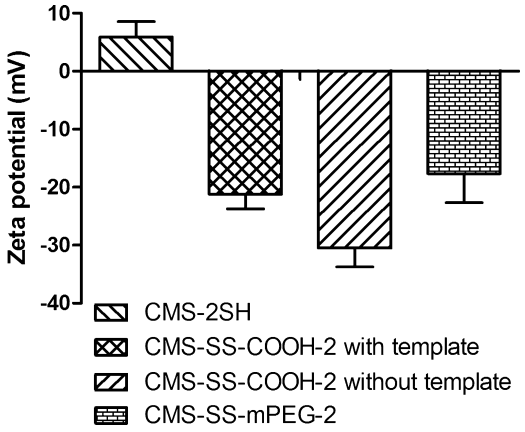

Fig. 6. The corresponding zeta potentials measured at each step of the drug loading process.

grafted onto the CMS *via* disulfide bonds, so the thiol-functionalized CMS carriers without template extraction were firstly reacted with Py—SS—COOH to allow the external thiol groups to be transformed into SS—COOH. Then, CMS—SS—COOH was refluxed to remove the template to allow the exposure of the internal thiols. Finally, 6-MP was loaded in the CMS—SS—COOH by a disulfide bond exchange reaction, followed by grafting of the mPEG to the outer surface of the silica by an esterification reaction.

The successful grafting and drug loading process was validated by a variety of methods. A comparison of the FT-IR spectra of CMS-2SH with the template, CMS—SS—COOH-2 after template extraction and CMS—SS—mPEG-2 are shown in Fig. 5. After the modification of CMS—SS—COOH, an additional adsorption peak appeared at 1720 cm^{-1}, which could be attributed to the C=O stretching vibration of the carboxyl group, indicating that the disulfide bond and terminal carboxyl group were successfully modified on the CMS nanoparticles. In addition, the surfactant removal process was confirmed by a reduction in the adsorption peaks around 2851 and 2923 cm^{-1}, which were attributed to the vibration of $-CH_2$. The remaining adsorption peaks at 2851 and 2923 cm^{-1} were likely due to the vibration of $-CH_2$ in the MPTMS. After grafting with mPEG, the adsorption peak at 1720 cm^{-1} disappeared, indicating the successful grafting of mPEG on the CMS surface by the esterification reaction. This result was also confirmed by the zeta potential characterization. As shown in Fig 6, the zeta potential of CMS-2SH without template extraction was +5.91 mV due to the cationic surfactant CTACl. The zeta potential was reversed to a negative one of −21.2 mV after the formation of CMS—SS—COOH due to the carboxyl groups produced on the surface of the CMS nanoparticles. Then, the zeta potential was further reduced to −30.5 mV after removal of the cationic surfactant. After the grafting of mPEG, the zeta potential increased to −17.6 mV, further supporting the results obtained from the FT-IR spectra.

3.3. Drug loading efficiency

The thiol-functionalized CMS carriers with the addition of different volumes of MPTMS were prepared to evaluate the effect of different amounts of modified thiol on the drug loading efficiencies and release properties. The loading efficiencies of 6-MP from CMS-SS-MP and CMS-SS-MP@mPEG samples are shown in Table 1. As can be seen from this table, when the added volume of MPTMS was 0.5 mL, the samples CMS-SS-MP-2 and CMS-SS-MP@mPEG-2 had the highest drug loading efficiency up to 4.95% and 4.07%, compared with their respective counterparts. However, with the increasing of the volume of MPTMS added from 0.75 mL to 1.00 mL, the drug loading efficiency decreased. The reason for this may be due to the contradiction between the modified amount of thiol and the pore size distributions of the functional silica.

The W_{BJH} of the carriers prepared with the addition of 0.25 mL MPTMS was 2.5 nm, a relatively larger aperture compared with that of the carriers that prepared with more MPTMS. However, the relatively low thiol modification on the internal and external surface of CMS resulted in a relatively low drug loading efficiency. When the added volume of MPTMS was 0.5 mL, the W_{BJH} of CMS deceased to ca. 2.2 nm, but it was still larger than the longest axis of the MP-SS-MP drug molecule (1.29 nm) as shown in Scheme 2. However, when the added volume of MPTMS was further increased to 0.75 mL or 1 mL, the W_{BJH} of CMS was reduced to the micropore range (<2.0 nm). Although the thiol content of CMS-3SH and CMS-4SH was more than that of CMS-2SH, there was not enough space for the thiol exchange reaction. In addition, during the drug loading process, the drug molecules gradually spread from the solvent to the internal pore channels of the carriers. The carrier pore channels were further reduced, when 6-MP was grafted to the carriers by disulfide bonds. For CMS-3SH and CMS-4SH carriers, with a pore size distribution in the micropore range, the internal pores might be blocked or become too small for the MP-SS-MP to diffuse into them, when 6-MP was grafted onto the external pores of the CMS carriers. Therefore, for CMS nanoparticles, when the volume of added MPTMS was 0.5 mL, the carrier had a suitable amount of modified thiol, and a relatively large pore size distribution at 2.2 nm.

The drug loading efficiency of CMS-SS-MP@mPEG samples was less than that of their counterparts without the grafting of mPEG because the modified thiol groups on the surface of CMS reacted with Py—SS—COOH. In addition, with an increasing volume of MPTMS, the reduced loading efficiency of CMS-SS-MP@mPEG samples compared with their counterparts was increased. The reason for this could be explained by the fact that the amounts of mercapto groups on the surface of the carrier were increased due to the increase in the added volume of MPTMS and, therefore, the amount of thiol groups reacting with Py—SS—COOH was also increased.

3.4. Redox-triggered drug release

The cumulative release curves of 6-MP from CMS-SS-MP, CMS-SS-MP@mPEG, and CMS-SH/MP samples are shown in Fig. 7A and B. The CMS-SH/MP sample (6-MP loaded in the carrier by noncovalent interaction) showed a rapid release with a cumulative release up to 80% within 0.5 h in the absence of GSH. In contrast, no premature leakages were observed from the prepared CMS-SS-MP and CMS-SS-MP@mPEG nanoparticles in the absence of GSH, regardless of the modified amount of thiol, indicating zero-release of 6-MP before the DDS reached the therapeutic site. However, when 3 mM GSH was added to the release fluids, all the 6-MP loaded samples with the drug conjugated to the silica by disulfide bonds exhibited redox-responsive release properties, and the cumulative release reached more than 70% within 2 h. The samples CMS-SS-MP-4 and CMS-SS-MP@mPEG-4 had the fastest dissolution rates but the lowest drug loading efficiency compared with their counterparts. When the added volume of MPTMS was 1 mL, the samples CMS-4SH and CMS—SS—COOH-4 had the highest amounts of modified thiol but the lowest S_{BET} and W_{BJH} (W_{BJH}<2.0 nm). So, 6-MP was mainly loaded on the external pores of CMS. Hence, for samples CMS-SS-MP-4 and CMS-SS-MP@mPEG-4, the loaded 6-MP could rapidly diffuse into the release media. However, for other loaded samples with the addition of different volumes of MPTMS, the cumulative release rates were not significantly different. The redox-responsive release properties are particularly important for drug delivery, especially for toxic

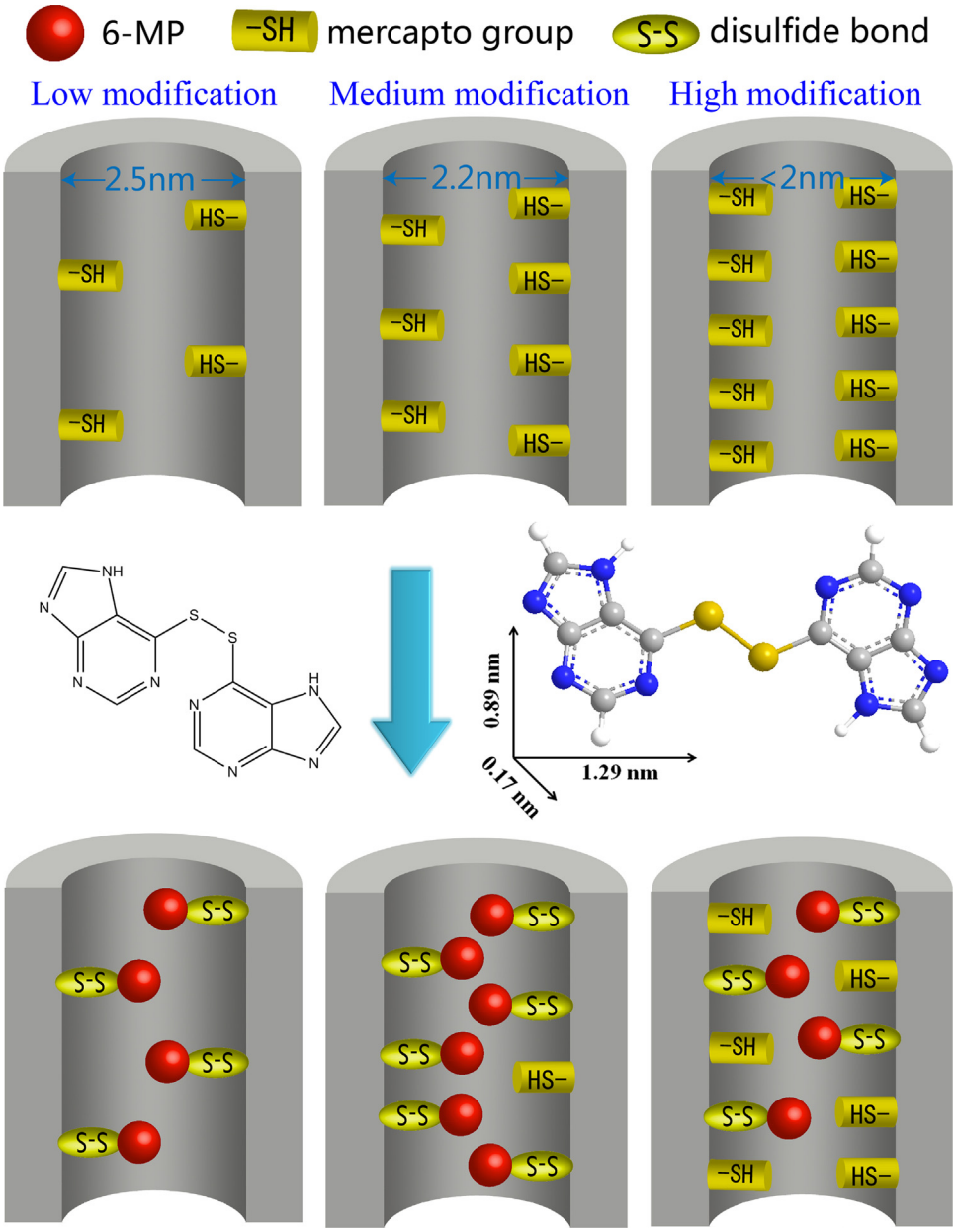

Scheme 2. Scheme of the impact on the different amounts of modified thiol on the drug loading efficiency. (The 3D structure of MP-SS-MP was simulated by ChemBioOffice software, which was used to draw and simulate chemical structures).

anticancer drugs. In addition, the cumulative release profiles of CMS-SS-MP@mPEG samples did not show any significant difference compared with their counterparts without grafting of mPEG, indicating that the hydrophilic PEG chains did not prevent drug release due to the cleavable disulfide bonds. Although the thiol groups on the surface of CMS were occupied by the grafting of mPEG, the dispersibility of CMS was improved due to the hydrophilic mPEG, which allowed full contact between the CMS nanoparticles and the GSH in the release medium.

3.5. The effect of grafting mPEG on the surface of CMS nanoparticles

One of the main problems associated with a variety of nanocarriers is that nanoparticles tend to agglomerate. Good dispersity of silica nanoparticles is essential for injection administration (Lin et al., 2011). Here, the dispersity of CMS-SS-mPEG nanoparticles was evaluated and compared with that of thiol-functionalized CMS. Nanoparticles of CMS-2SH and CMS-SS-mPEG-2 in ethanol suspensions were dried by vacuum filtration and redispersed by ultrasonication in distilled water for 15 min. As shown in Table 3, the mean hydrodynamic diameter of CMS-2SH before drying was 161 nm, larger than the result observed from SEM due to the hydrated layer in the aqueous environment. However, the hydrodynamic diameter of CMS-2SH was increased to 354 nm with a Polydispersity (PDI) of 0.358 after drying. In contrast, the mean hydrodynamic diameter of CMS-SS-mPEG-2 was only slightly increased and the PDI was still less than 0.2 after drying, indicating that CMS-SS-mPEG-2 had a better dispersibility in water due to the grafting of hydrophilic mPEG chains on the surface of CMS.

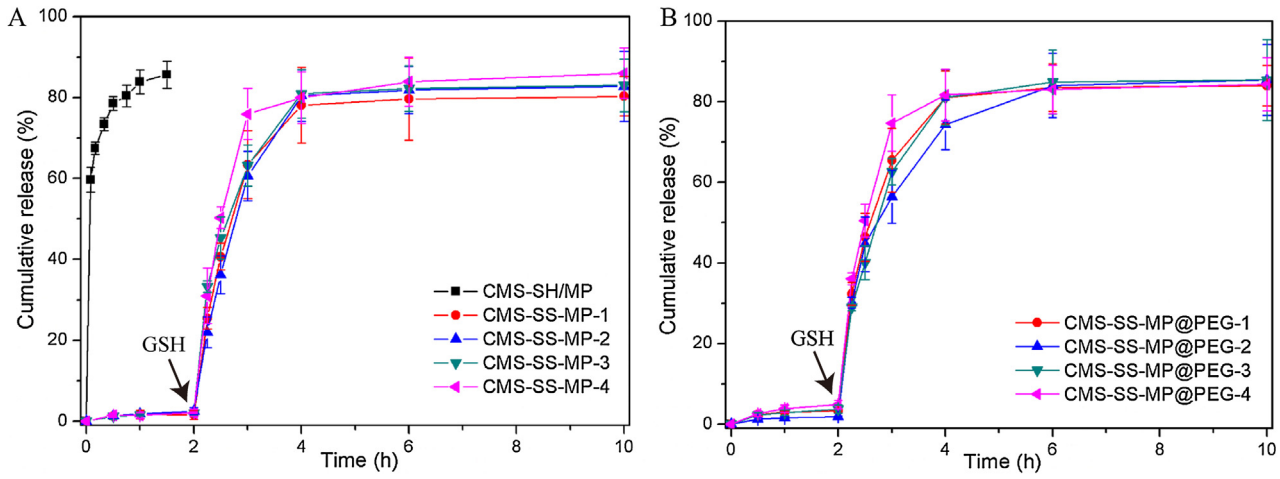

Fig. 7. Cumulative release profiles of 6-MP from (A) CMS-SS-MP samples and CMS-SH/MP, and (B) CMS-SS-MP@mPEG in pH 7.4 PBS in the presence or absence of 3 mM GSH.

Table 3
The changes of mean hydrodynamic diameter and polydispersity of CMS and CMS-SS-mPEG nanoparticles in water before and after drying.

Particles type	CMS-2SH		CMS-SS-mPEG-2	
	Before drying	After drying	Before drying	After drying
Mean hydrodynamic diameter (nm)	161 ± 9	354 ± 80	193 ± 9	216 ± 41
Polydispersity	0.152 ± 0.031	0.358 ± 0.87	0.092 ± 0.020	0.165 ± 0.031

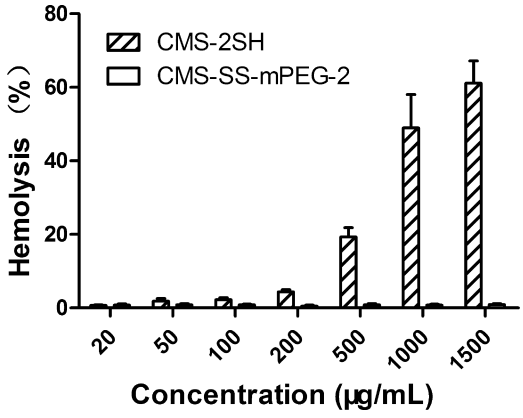

Fig. 8. Hemolysis of the CMS-2SH and CMS-SS-mPEG-2 at different concentrations.

The adsorption of BSA to the surface of the CMS nanoparticles was measured to evaluate the effectiveness of mPEG modification. It was found that mPEGylated CMS nanoparticles sharply reduced the BSA adsorption from 2.14 wt.% (CMS-2SH) to 0.54 wt.% (CMS-SS-mPEG-2). It is accepted that the steric repulsion force of mPEG chains could play an important role in preventing BSA adsorption onto the nanoparticles and reduce the rate of clearance, thus increasing the circulation time of nanoparticles for *in vivo* applications.

The hemolysis assay was used to evaluate the cytotoxic effect of the silica materials for *in vivo* applications The percentage hemolysis of CMS-2SH and CMS-SS-mPEG-2 samples is shown in Fig. 8. The percentage hemolysis of the bare CMS-2SH samples increased in a concentration-dependent manner over a wide concentration range of 20–1500 μg/mL. When the concentration of bare CMS-2SH reached 500, 1000, and 1500 μg/mL, the percentage hemolysis was 19.3%, 48.9%, and 61.1%, respectively. Unlike bare CMS-2SH, no hemolysis was seen for the CMS-SS-mPEG-2 sample, even at a high nanoparticle concentration (1500 μg/mL). This reason for this might be mainly due to the modification of biocompatible mPEG chains on the surface of silica which can significantly decrease the reactive oxygen species (ROS) induced by the surface of silanol groups and electrostatic interactions between silica and membrane proteins (Nash et al., 1966; Slowing et al., 2009). This result demonstrated that the mPEG modification on the surface of CMS could improve the biocompatibility of silica when administered intravenously. The above results suggest that the hydrophilic mPEG chains can dramatically reduce the percentage hemolysis and protein adsorption, and increase the dispersibility and biocompatibility of CMS nanoparticles.

4. Conclusions

In summary, a redox-responsive delivery system based on CMS has been developed to load thiol-containing or thiolated drugs *via* cleavable disulfide bonds, in which mPEG was conjugated on the surface of silica by disulfide bonds. The CMS carriers with different amounts of thiol groups were prepared to evaluate the effect of different amounts of modified thiol on the drug loading efficiencies. The *in vitro* release results demonstrated that the redox-responsive DDS exhibited “zero” premature release in the absence of GSH, and the cumulative release reached more than 70% within 2 h in the presence of 3 mM GSH. Also, the hydrophilic mPEG did not prevent drug release due to the cleavable disulfide bonds and the improved dispersibility. In addition, mPEG increased the biocompatibility and dispersibility of CMS nanoparticles by reducing the degree of hemolysis and protein adsorption when administered intravenously. This work provides a new strategy to link bioactive drugs and hydrophilic polymers to the interiors and exteriors of MSN *via* disulfide bonds to obtain redox-responsive release.

Acknowledgements

This work was supported by National Basic Research Program of China (973 Program) (NO. 2015CB932100), National Natural Science Foundation of China (NO. 81473165).

References

Ahn, B., Park, J., Singha, K., Park, H., Kim, W.J., 2013. Mesoporous silica nanoparticle-based cisplatin prodrug delivery and anticancer effect under reductive cellular environment. J. Mater. Chem. B 1, 2829–2836.

Chen, W., Zhong, P., Meng, F., Cheng, R., Deng, C., Feijen, J., Zhong, Z., 2013. Redox and pH-responsive degradable micelles for dually activated intracellular anticancer drug release. J. Control. Release 169, 171–179.

Cheng, R., Feng, F., Meng, F., Deng, C., Feijen, J., Zhong, Z., 2011. Glutathione-responsive nano-vehicles as a promising platform for targeted intracellular drug and gene delivery. J. Control. Release 152, 2–12.

Cui, Y., Dong, H., Cai, X., Wang, D., Li, Y., 2012. Mesoporous silica nanoparticles capped with disulfide-linked peg gatekeepers for glutathione-mediated controlled release. ACS Appl. Mater. Interfaces 4, 3177–3183.

Duan, X., Xiao, J., Yin, Q., Zhang, Z., Yu, H., Mao, S., Li, Y., 2013. Smart ph-sensitive and temporal-controlled polymeric micelles for effective combination therapy of doxorubicin and disulfiram. ACS Nano 7, 5858–5869.

Giri, S., Trewyn, B.G., Stellmaker, M.P., Lin, V.S.Y., 2005. Stimuli-responsive controlled-release delivery system based on mesoporous silica nanorods capped with magnetic nanoparticles. Angew. Chem. Int. Ed. 44, 5038–5044.

Gu, J., Su, S., Zhu, M., Li, Y., Zhao, W., Duan, Y., Shi, J., 2012. Targeted doxorubicin delivery to liver cancer cells by PEGylated mesoporous silica nanoparticles with a pH-dependent release profile. Micropor. Mesopor. Mater. 161, 160–167.

He, D., He, X., Wang, K., Cao, J., Zhao, Y., 2012. A light-responsive reversible molecule-gated system using thymine-modified mesoporous silica nanoparticles. Langmuir 28, 4003–4008.

He, Q., Zhang, J., Shi, J., Zhu, Z., Zhang, L., Bu, W., Guo, L., Chen, Y., 2010. The effect of PEGylation of mesoporous silica nanoparticles on nonspecific binding of serum proteins and cellular responses. Biomaterials 31, 1085–1092.

Kim, T.-W., Slowing, I.I., Chung, P.-W., Lin, V.S.-Y., 2010. Ordered mesoporous polymer-silica hybrid nanoparticles as vehicles for the intracellular controlled release of macromolecules. ACS Nano 5, 360–366.

Lai, C.-Y., Trewyn, B.G., Jeftinija, D.M., Jeftinija, K., Xu, S., Jeftinija, S., Lin, V.S.-Y., 2003. A mesoporous silica nanosphere-based carrier system with chemically removable CdS nanoparticle caps for stimuli-responsive controlled release of neurotransmitters and drug molecules. J. Am. Chem. Soc. 125, 4451–4459.

Langer, R., 1998. Drug delivery and targeting. Nature 392, 5–10.

Lee, C.H., Cheng, S.H., Huang, I., Souris, J.S., Yang, C.S., Mou, C.Y., Lo, L.W., 2010. Intracellular pH-responsive mesoporous silica nanoparticles for the controlled release of anticancer chemotherapeutics. Angew. Chem. 122, 8390–8395.

Lin, Y.-S., Abadeer, N., Hurley, K.R., Haynes, C.L., 2011. Ultrastable, redispersible, small, and highly organomodified mesoporous silica nanotherapeutics. J. Am. Chem. Soc. 133, 20444–20457.

Lu, F., Wu, S.H., Hung, Y., Mou, C.Y., 2009. Size effect on cell uptake in well-suspended: uniform mesoporous silica nanoparticles. Small 5, 1408–1413.

Möller, K., Kobler, J., Bein, T., 2007. Colloidal suspensions of mercapto-functionalized nanosized mesoporous silica. J. Mater. Chem. 17, 624–631.

Nash, T., Allison, A., Harington, J., 1966. Physico-chemical properties of silica in relation to its toxicity. Nature 210, 259–261.

Park, C., Kim, H., Kim, S., Kim, C., 2009. Enzyme responsive nanocontainers with cyclodextrin gatekeepers and synergistic effects in release of guests. J. Am. Chem. Soc. 131, 16614–16615.

Saito, G., Swanson, J.A., Lee, K.-D., 2003. Drug delivery strategy utilizing conjugation via reversible disulfide linkages: role and site of cellular reducing activities. Adv. Drug Deliv. Rev. 55, 199–215.

Slowing, I.I., Wu, C.W., Vivero-Escoto, J.L., Lin, V.S.Y., 2009. Mesoporous silica nanoparticles for reducing hemolytic activity towards mammalian red blood cells. Small 5, 57–62.

Soppimath, K.S., Aminabhavi, T.M., Kulkarni, A.R., Rudzinski, W.E., 2001. Biodegradable polymeric nanoparticles as drug delivery devices. J. Control. Release 70, 1–20.

Torchilin, V.P., 2005. Recent advances with liposomes as pharmaceutical carriers. Nat. Rev. Drug Discov. 4, 145–160.

Wang, L.-S., Wu, L.-C., Lu, S.-Y., Chang, L.-L., Teng, I.-T., Yang, C.-M., Ho -a, J.A., 2010. Biofunctionalized phospholipid-capped mesoporous silica nanoshuttles for targeted drug delivery: improved water suspensibility and decreased nonspecific protein binding. ACS Nano 4, 4371–4379.

Wang, X., Cai, X., Hu, J., Shao, N., Wang, F., Zhang, Q., Xiao, J., Cheng, Y., 2013. Glutathione-triggered off-on release of anticancer drugs from dendrimer-encapsulated gold nanoparticles. J. Am. Chem. Soc. 135, 9805–9810.

Zhao, Y., Vivero-Escoto, J.L., Slowing, I.I., Trewyn, B.G., Lin, V.S., 2010. Capped mesoporous silica nanoparticles as stimuli-responsive controlled release systems for intracellular drug/gene delivery. Expert Opin. Drug Deliv. 7, 1013–1029.